**ORIGINAL ARTICLE**

# Thermo-electric modeling and analysis of lithium-ion battery pack for E-mobility

Mahipal Bukya[1,2] · Rajesh Kumar[2] · Akhilesh Mathur[2] · Din Bandhu[3] · V Suryaprakash Reddy[4]

**Abstract**

Electric Vehicles (EVs) have emerged as a viable and environmentally sustainable alternative to traditional internal combustion vehicles by utilizing a clean energy source. The advancement and expansion of electric cars rely on the progress of electrochemical batteries. The utilization of Lithium-Ion Batteries is widespread primarily because of its notable energy density. Changes influence the performance of these batteries in temperature. The Thermal Management System of the battery is one of the very important systems in EVs to improve the performance and life of the battery. The geometrical spacing of the cell modules is considered identical for a more accurate comparison of temperature distribution. For better cooling and heat dissipation, the battery pack's two sides are kept entirely open to facilitate the inflow of air. In this work, active BTMS solutions are selected and analyzed using the development of three-dimensional free, open-source OpenFOAM computational fluid dynamics simulations for accurate thermal modeling and hotspot zones in cylindrical battery packs. The outcome of the simulations is compared using parameters like temperature distribution in battery cells, battery modules, and heat generation. Among all the cell temperature zones, the temperature maximum is near the sixth cell of the module depth. OpenFOAM results validated with the existing literature's experimental and Ansys results. Air cooling is utilized for cooling performance because of its relatively simple structure and lightweight.

## List of symbols

| | |
|---|---|
| $Q_{joule}$ | Joule heating (joules per second) |
| $Q_{entropic}$ | Entropic heating (joules per second) |
| $V$ | Cell potential (Volt) |
| $V_o$ | Open circuit potential (Volt) |
| $R$ | The internal resistance of battery cell ($\Omega$) |
| $I$ | Current (Amp) |
| $h$ | Convective heat transfer coefficient (W/m$^2$K) |
| $L_c$ | Characteristics length (m) |
| $Bi$ | Biot number (-) |
| $T_{cell}$ | Instantaneous cell temperature ($^o$C) |
| $K_b$ | Thermal conductivity, W/mK |
| $C$ | Discharge rate |
| $Cp,b$ | Specific heat (J/kg K) |
| $L$ | Length (mm) |
| $\rho_b$ | Density (kg/m3) |
| $D$ | Diameter (mm) |
| $t$ | Time (s) |
| $W$ | Vertical length (mm) |
| $L$ | Horizontal length (mm) |
| $A_s$ | Area of a single battery cell (m2) |
| $Q_{gen}$ | Heat generation in a cell (J/s) |
| $V_b$ | Volume of a single battery cell (m3) |
| $m$ | Mass of a cell (kg) |

✉ Din Bandhu
din.bandhu@manipal.edu

1 Department of Electrical and Electronics Engineering, Manipal Institute of Technology Bengaluru, Manipal Academy of Higher Education, Manipal 576104, India

2 Department of Electrical Engineering, Malaviya National Institute of Technology, Jaipur 302017, India

3 Department of Mechanical and Industrial Engineering, Manipal Institute of Technology Bengaluru, Manipal Academy of Higher Education, Manipal 576104, India

4 Department of Civil Engineering, Institute of Aeronautical Engineering, Hyderabad, Telangana 500043, India

## Abbreviations

| | |
|---|---|
| BP | Battery pack |

| EV | Electric vehicle |
| HEVs | Hybrid electric vehicles |
| PHEVs | Plug-in hybrid electric vehicle |
| PCM | Phase-change material |
| Li-ion | Lithium ion |
| UDF | User defined function |
| SOC | State of charge |
| CFD | Computational fluid dynamics |
| BTMS | Battery thermal management system |
| OpenFOAM | Open field operation and manipulation |

# 1 Introduction

The worldwide shift towards sustainable transportation solutions has catalyzed the exponential expansion of EVs as a viable substitute for conventional internal combustion engine automobiles. Nevertheless, with the ongoing acceleration in the adoption of EVs, there has been a shift in attention towards the need to guarantee the long-term sustainability of EV operations on a global scale. Currently, the advancement of EVs stands as the most auspicious resolution. The prevalence of LIB in contemporary EVs may be attributed to its notable attributes, including high energy density, efficiency, and longevity [1–3]. Consequently, the performance of these batteries plays an important role in determining the range, fuel efficiency, and power capabilities of EVs. Nevertheless, the quick charging and discharging of a battery can result in significant heat generation, hence posing a potential hazard of battery overheating and combustion, affecting on insulation strength of the battery as well as the neighboring cabling network, and even explosion if the dissipation of the created heat is not promptly addressed. The recommended operational temperature range for a single battery is documented to be between 25 and 40°C [4, 5]. Additionally, it is advised to maintain the most temperature difference of 5 °C between the individual cells inside the battery module. The detrimental impact on battery performance and lifespan might be attributed to immoderate battery temperature or an unbalanced temperature distribution inside the battery pack module.

Currently, a significant issue arising from the elevated temperatures of LIB is the occurrence of thermal runaway. Thermal runaway is a phenomenon characterized by an accelerated increase in temperature, leading to detrimental outcomes such as fast temperature escalation, gas production, and potentially even battery detonation. This phenomenon exerts a detrimental impact on both the safety of cars and the well-being of passengers. The BTMS of the battery is one of the very important components in an electric vehicle, intending to improve the battery's performance and life. BTMS

should ensure features such as good performance, simplicity, less weight, low cost, low use of parasitic power and fast packaging, no harmful gas emissions, and easy maintenance. There are different battery cooling methods and solutions used in BTMS shown clearly in Fig. 1.

The Active BTMS has been considered for the cooling performance of the battery pack, an air cooling system uses natural air or fans to direct airflow to cool. Air is straightforwardly available for cooling purposes and it is broadly used in many industries because of its relatively simple structure, low cost, being the most straightforward, safe, and reliable in its operation; ease of maintenance and implementation, and its lightweight. In the liquid direct cooling system, the battery is submerged directly into the coolant, with direct liquid contact with cells to maximize the heat absorptions, it's have highest heat capacity but needs a design that can prevent leakage and spill. The weight of the BTMS is also more as compared to active BTMS. Requires coolant to be low to no conductivity to maintain vehicle safety increasing R&D efforts across industries [6–8]. In the liquid indirect cooling system, the cell is in contact with a sink through which liquid flows to absorb heat. Even if it has better heat capacity, direct contact with the portion of the cell does not allow uniform heat dissipation. Coolant circulates through a system of pipes, similar to the cooling system found in current IC engines. Requires high heat capacity coolants with corrosion inhibitors. In Phase Change Materials (PCM) cooling system is effective in cooling function but requires large volume space. Phase change composites are being commercialized across material handling, energy storage, and transportation. The benefits and drawbacks of the proposed works of literature [9–12] BTMS solutions are thoroughly examined, as well as the adaptability of these systems.

In literature [13], notable work has been done on battery thermal distribution where it has been mentioned that the middle of the second row has the maximum temperature. Some researchers reported that the maximum temperature is observed nearest to the positive terminal [14] while others reported that it appears in the electrode region [15]. Considering all these factors and applying the highly thin meshing to electrode regions because of its faces the more current carrying zones so heat will be more. The cell-wise average temperature was also considered at 500 s to predict the highest heating zones of cells, a nodal and elemental average of the case has been performed to reduce the errors and considered the triangular type meshing. The most heat-facing cells in the battery modules are identified near to last row of the middle cell. The purpose of this paper is to critically evaluate previous studies and research on the types, and designs, showing the simulated generation of heat and the distribution of temperature throughout the battery pack module and operating principles of BTMSs
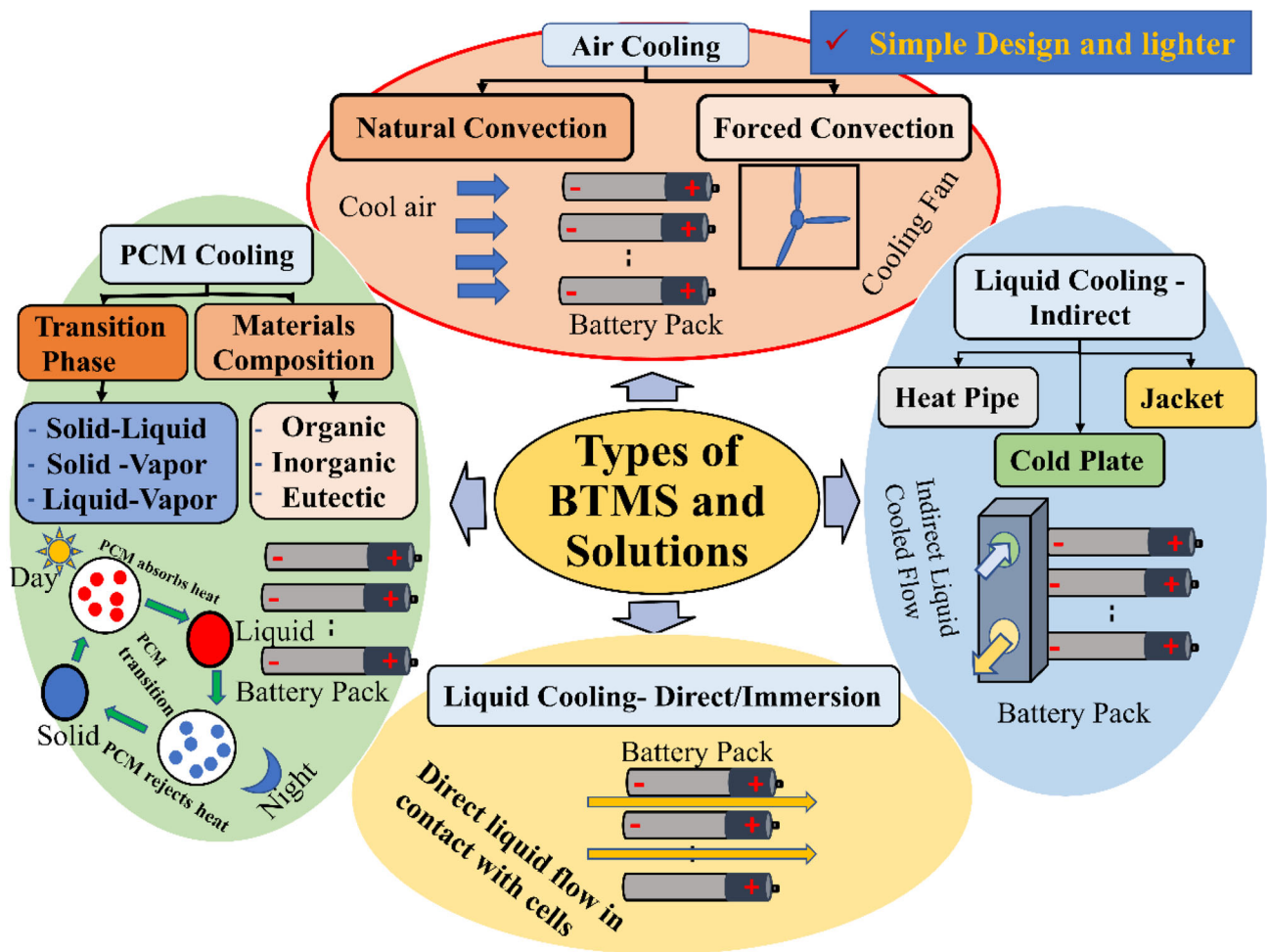
**Fig. 1** Types of BTMS and its solutions

used in the building of cylindrical-shaped LIBs by using free software Open FOAM CFD which is freely available online, with a focus on cooling methods. Also analyzed are the thermal runaway behavior and the resulting regimes in cylindrical battery pack modules, as well as the battery flow field. Experimental and Ansys data from the available literature [13, 14] were used to verify the open FOAM results.

The rest of this study is organized as follows: Sect. 2 discusses Materials and Methods introducing the battery pack thermal management system. It further discusses the battery thermal modeling and numerical approach. Section 3 discusses the results and discussions in detail and Sect. 4 presents the conclusion of the research.

## 2 Material and methods

### 2.1 Design procedure

The performance of a battery system is influenced by various factors, including temperature, time, state of charge, and condition of health. These factors have a direct impact on the generation of electricity, electrochemical reactions, and heat transfer inside the battery system. However, it is important to note that these effects mostly impact the battery when subjected to high discharge rates, generally above 1 °C. Consequently, they have the potential to generate non-uniform temperature distributions within the battery, ultimately leading to a decrease in its overall lifespan [15, 16]. It is currently inevitable to encounter temperature variations within the battery cell when subjected to high discharge rates [17, 18]. There are varying findings among researchers on the location of the maximum temperature. Some studies indicate that it is recorded close to the positive terminal [19–21], but others suggest that it is found in the electrode region [22].
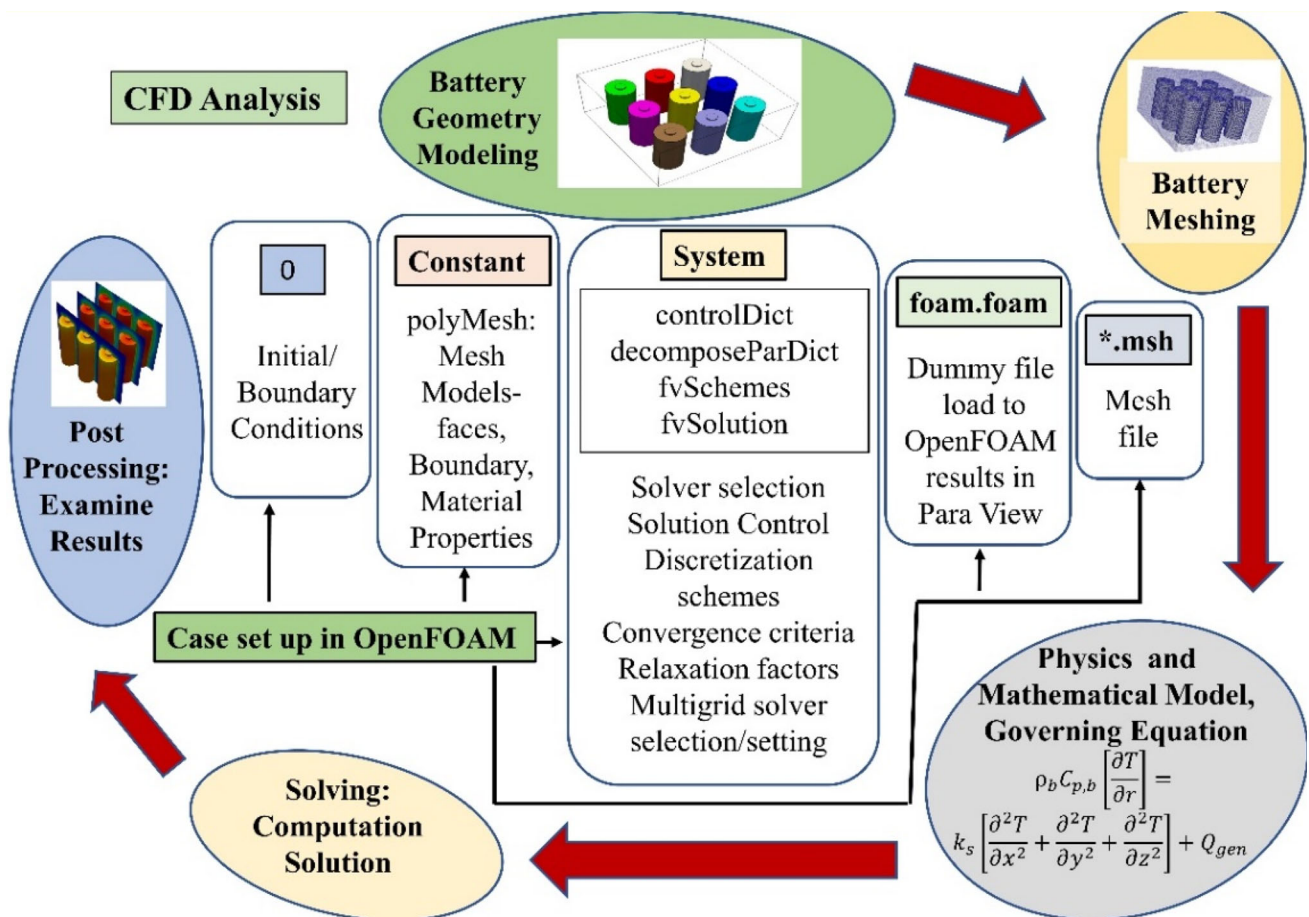
**Fig. 2** Steps to perform CFD Analysis

Furthermore, subjecting a Li-ion cell to a rapid decrease in temperature can negatively impact the temperature differentials [23]. Currently, researchers are engaged in efforts to address the issue of geographical variability in temperature increases intending to optimize cell operation. The battery cells possess a possible susceptibility to thermal runaway. Thermal runaway is a phenomenon that typically arises in the context of an exothermic reaction, specifically during the charging or discharging phase [24]. This occurrence is commonly observed when a short circuit condition is present [25]. The aforementioned circumstance can induce a substantial increase in temperature within the cell, reaching a maximum of 500 °C [26]. Consequently, this thermal escalation poses a risk of detrimental effects on both the individual cell and the overall functionality of the battery pack. The latest advancements in cell technology have resulted in a decrease in elevated temperatures. However, despite these improvements, there remains a possible concern regarding thermal runaway, which can be attributed to the quick charging process and repeated working cycles [27–30]. The steps involved in CFD analysis have been depicted in Fig. 2.

The heat-generating characteristics of the batteries and the thermal storage/distribution properties are the two most crucial factors to consider when designing a TMS for lithium-ion battery packs. The PVC film, the steel shell, and the battery core make up the three components of the battery model. The battery core is an anisotropic material, whereas the PVC film and steel shell are isotropic materials in terms of thermal conductivity [31, 32]. This study considered the cylindrical cell battery pack, examined the transient thermal behavior of cylindrical Li-ion battery modules when cooled by forced air, and accounted for the heat exchange between the individual cells. When designing the BTMS for a high-discharge-rate, air-cooled battery pack, it is crucial to have a firm grasp on such design considerations as the transient thermal response, the evolution of flow fields and temperature regimes, the existence of temperature inhomogeneities between individual cells, and the positioning of hotspots. For comparison with OpenFOAM CFD results, the maximum cell-to-cell temperature non-uniformity in the examined BTMS [13] is limited to 0.11 C and the battery temperature is less than 29 C despite the high discharge rate and decreased cooling airflow condition. The boundary conditions in this study are as follows: A
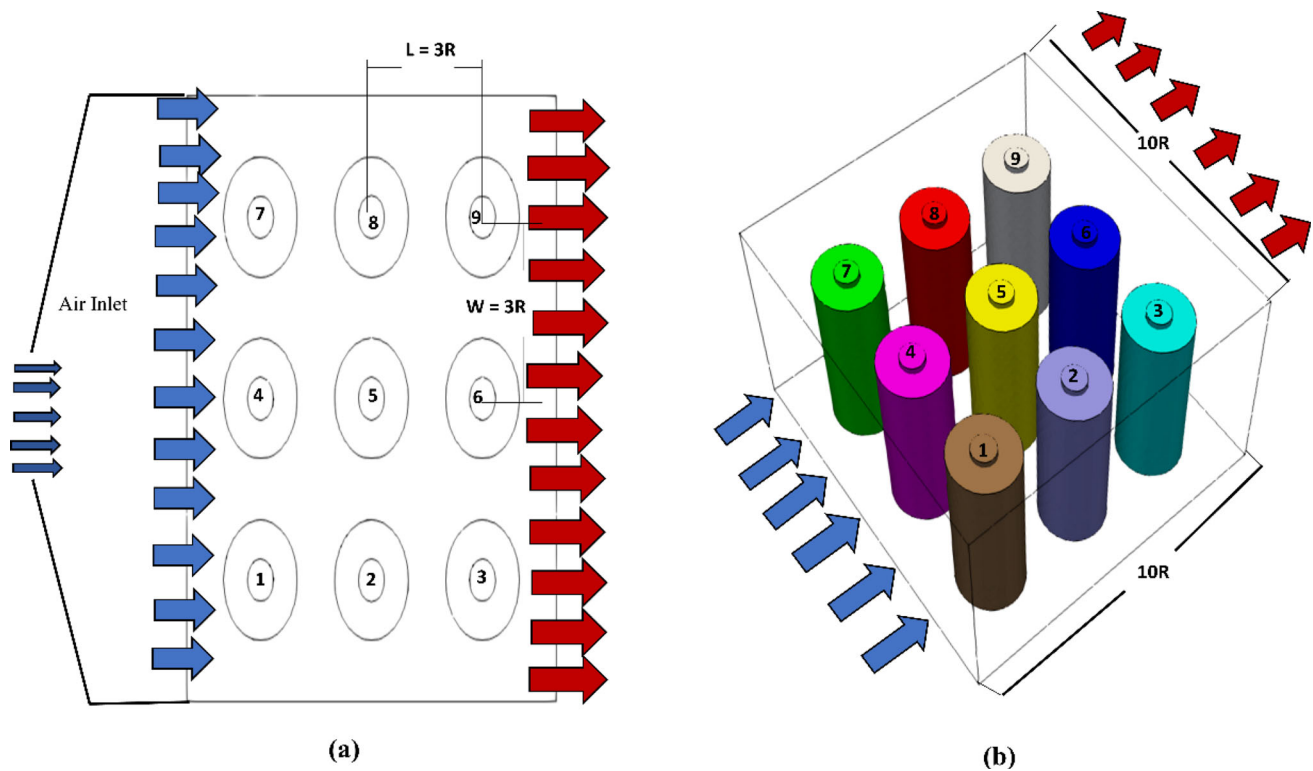
**Fig. 3** Battery pack dimensions: **a** Battery cells indices **b** Battery module under consideration

steady forced flow with a certain temperature at the inlet and free flow at the outlet. For optimal heat dissipation, the battery module is completely permeable on both the inflow and the outflow sides of the airflow direction. More space between cells is thought to improve cooling airflow and facilitate the venting of battery-generated gases [13, 33]. Nine cylindrical Li-ion cells, whose dimensions were obtained from the literature for comparison [9], make up the battery module. Each cell's neighboring distance, measured in both horizontal (L) and vertical (W) dimensions, is 3R and the battery module maintains a constant 10R in both width and depth. The dimensions can be seen from Fig. 3a cylindrical battery pack module and Fig. 3b battery cell indices are under consideration for building the simulation setup in OpenFOAM software. The airflow direction considered in this module is from left to right in the X-plan.

Table 1 details the Li-ion cell's thermophysical and chemical characteristics used for creating the case file of the simulation. Material in the battery pack is assumed to be isotropic, and the cells are treated as a single entity with constant thermal conductivity and specific heat [9, 34].

The mesh system was generated in the free OpenFOAMm CFD software. A three-dimensional finite element model of the battery pack module was modeled in OpenFOAM CFD using a variety of mesh sizes, including coarse, fine meshes and extra fine meshes of cylindrical batteries shown

**Table 1** Battery model parameters

| Item | Specification |
| --- | --- |
| Cell type | Cylindrical type |
| Number of cells | 9 |
| Current capacity | 3.6 Ah |
| Thermal conductivity ($K_b$) | 1.0 (radial direction) W/mK |
| Specific heat ($C_{p,b}$) | 837.4 J/kg K |
| Mass of cell | 0.3 kg |
| Diameter (D) | 42.4 mm |
| Density ($\rho_b$) | 2007.7 kg/m$^3$ |
| Length (L) | 97.7 mm |

in Fig. 4. The fine meshes considered for accurate simulation and fewer errors and extra fine meshes applied at the electrodes for accurate evaluation of temperature distribution. To test grid sensitivity, the battery module was modeled with several mesh sizes (mesh 1: 211,704 cells and 46,958 nodes, mesh 2: 1,453,695 cells and 287,013 nodes, mesh 3: 881,976 cells and 170,831 nodes) in Fig. 4.

Figure 5 depicts the computational mesh findings. After improving the mesh, it is possible to show that the solutions are grid-independent. To prevent the long computing time and solution instability, mesh 1 (211,704 cells and 46,958 nodes) was used.
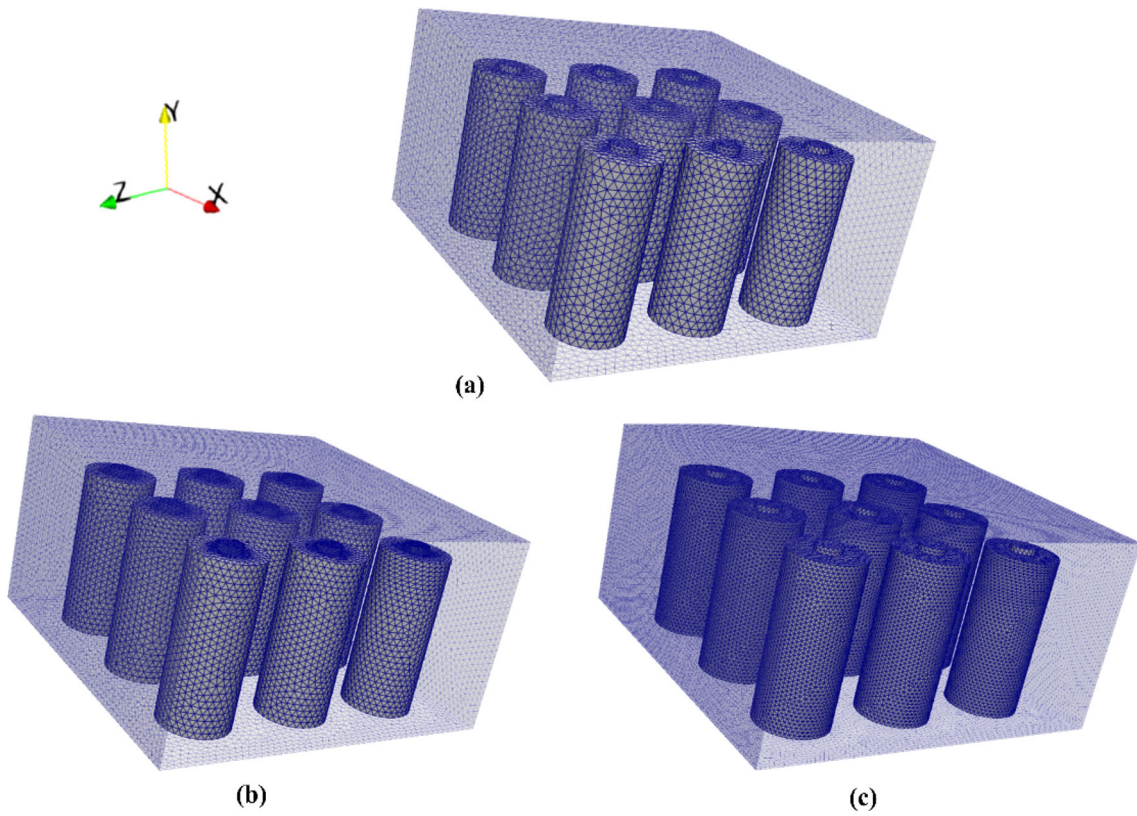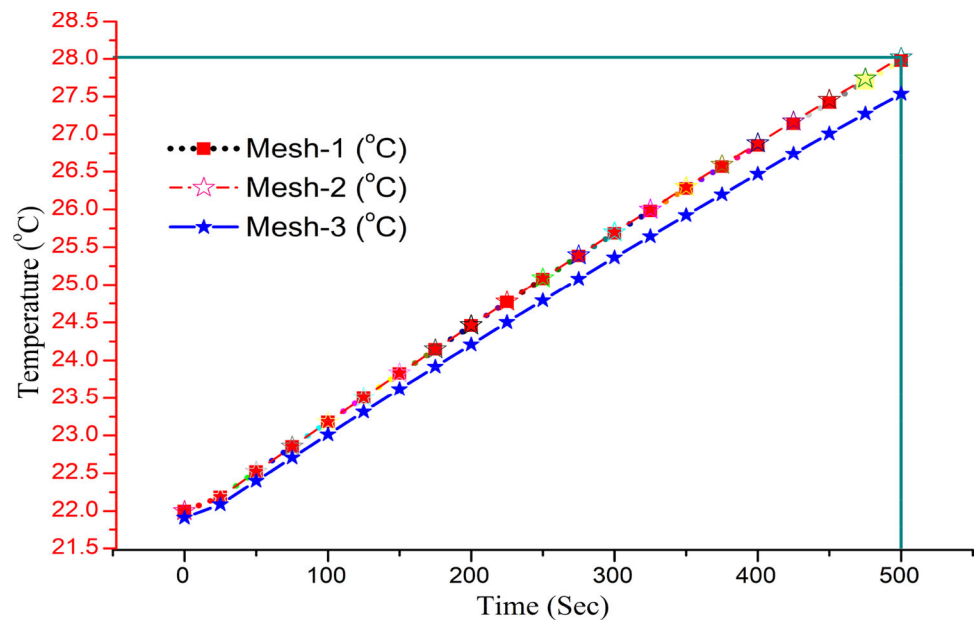
**Fig. 4** Analyzed mesh sizes **a** Coarse mesh, **b** Medium mesh, **c** Fine mesh, and extra fine mesh at electrodes of the battery

**Fig. 5** Mesh sensitivity of cylindrical battery pack module

## 2.2 Battery thermal modelling and numerical approach

The cooling of batteries exhibits a direct relationship with the amount of heat produced inside. Consequently, it is imperative to ascertain the sources of heat generation. Bernardi et al. employed a thermodynamic energy balance approach to derive a mathematical expression for the amount of heat produced within a battery. The author examines four distinct processes that impact this equilibrium [35]. There are two primary sources of energy within a battery: electrical power generation and reversible processes accompanied by entropic heating. The third stage involves the generation of heat resulting from the mixing process, which occurs due to the changing concentration of the batteries as the reaction progresses. The final stage in the energy balance pertains to the dissipation of heat resulting from the phase transitions of the materials. In this statement, the effects of heat of mixing and phase change are disregarded. The initial term in Eqs. (1–2) signifies the combined effects of overpotentials occurring during charge transfer at the contact and ohmic losses. The second term represents the reversible entropic heat generated by the process in Eq. (3) [34–40]. Both the irreversible effect of joule heating ($q_{joule}$) from the source resistance and the reversible effect of entropic change ($q_{entropic}$) are associated with the concept of heat generation ($q_{gen}$) in Li-ion batteries given by Eq. (1) [13, 16, 41].

$$q_{gen} + q_{entropic} + q_{joule} \tag{1}$$

The cell's source resistance and the related electrochemical reactions are responsible for the creation of joule heating, also known as a gradient potential, which is always interpreted as a positive quantity [17, 42]. The entropy of the process is what causes heat while charging and discharging. Depending on whether endothermic or exothermic events occur, it might have a positive or negative value. It is possible to calculate the amount of heat produced by joule heating using below Eq. (2):

$$q_{joule} = I(\phi - \phi_{oc}) = I^2 R \tag{2}$$

Here I is the current during the charging or discharging process, $\phi$ and $\phi_{oc}$ are cell potentials and open circuit potential, respectively. The source resistance (R) depends on the cell temperature ($T_{cell}$) [9, 13, 43] and can be expressed by Eq. (3).

$$R = -0.0001.T_{cell}^3 + 0.0134.T_{cell}^2$$
$$+ 0.5345.T_{cell} + 12.407 \quad (m\ddot{} ) \tag{3}$$

Here R is the resistance substituted milli ohms and cell temperature is in °C. The entropic heat generation is calculated by Eq. (4).

$$q_{entropic} = -I T_{cell} \frac{d\phi_{oc}}{dT} \tag{4}$$

Here $T_{cell}$ is the temperature of the cell. User-defined function (UDF) OpenFOAM coded function object is written based on Eqs. (1)–(4) for cylindrical battery pack cell heat generation. The numerical technique and validation utilize a simplified model of battery heat generation. Constant values for thermal conductivity and other physical properties can be employed in this case, as the selected battery material exhibits isotropy. The aforementioned equation is employed under the assumption that the temperature within the cellular environment remains constant. Hence, the utilization of a lumped capacitance model is necessary to ensure precise application of the equation. The Biot number (Bi) is employed in the field of heat transfer theory to evaluate the validity of this assumption. The dimensionless number denoted in this context represents the ratio between internal heat transfer and exterior heat transfer concerning internal conduction, as defined by Eq. (5) [14, 44].

$$Bi = \frac{h L_c}{k_b} \tag{5}$$

Here h is the convective heat transfer related to the cooling medium (air), $k_b$ represents the thermal conductivity of the battery material, and $L_c$ represents the characteristics length that was derived by Eq. (6).

$$Lc = \frac{V_b}{A_s} \tag{6}$$

The abbreviations "Vb" and "As" represent the volume and area, respectively, of an individual battery cell. The upper and lower surfaces of the battery cell are excluded from the calculation of the overall surface area. The OpenFOAM computational fluid dynamics (CFD) software is employed to generate and mesh a three-dimensional (3D) representation of a battery module. The software possesses several applications and can effectively address a diverse range of difficulties, encompassing intricate fluid dynamics involving chemical processes, turbulence, and heat transport, alongside challenges in acoustics, solid mechanics, and electromagnetics.

The increase in the interior temperature of the battery is a consequence of the governing equations that are required to uphold energy balance. Consequently, the temperature of the battery can be controlled by modulating the pace at which thermal energy is dissipated into the surrounding environment. The rate at which the temperature of the battery
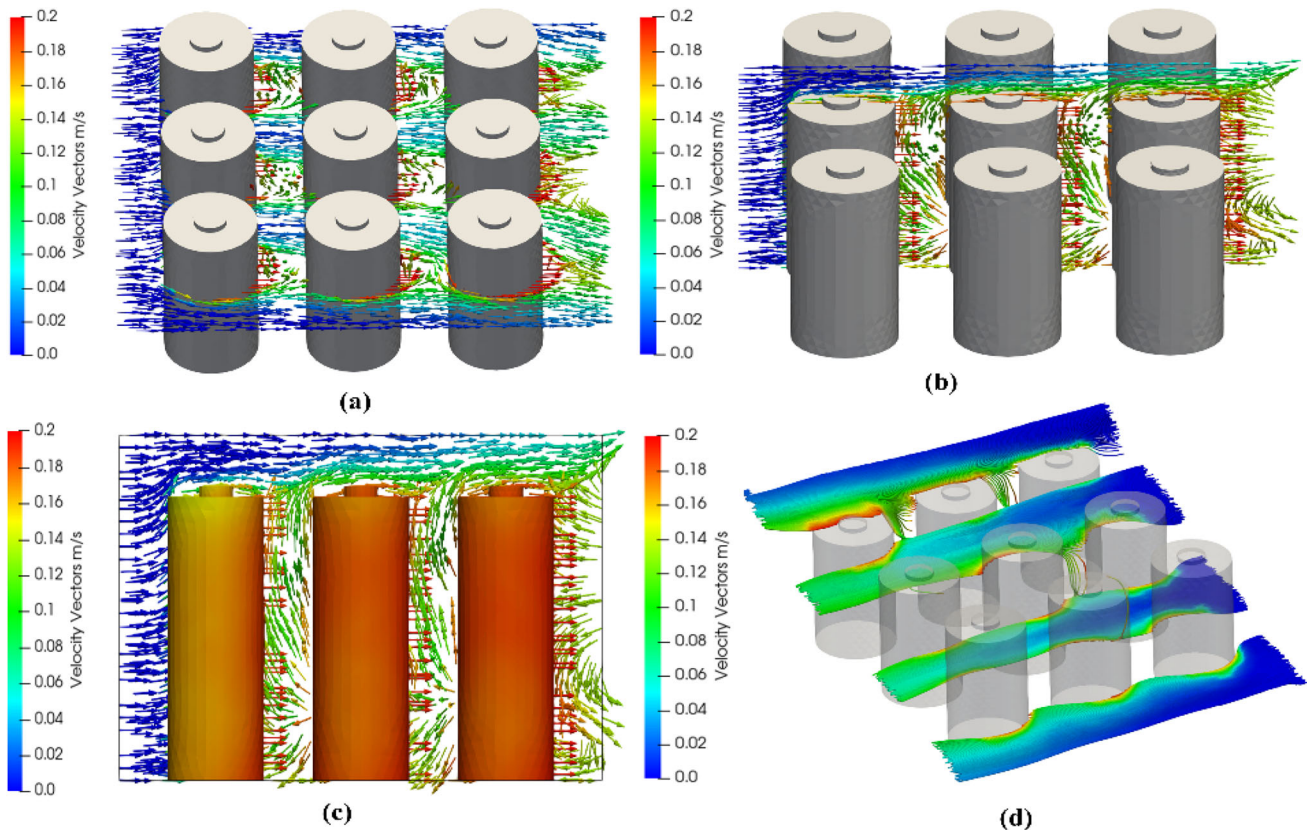
**Fig. 6** Variation in air temperature with flow direction

increases will be reduced if a greater amount of heat is dissipated. Hence, it is imperative to accurately formulate the energy balance equation, encompassing heat generation and heat transmission, while considering suitable boundary conditions, to predict the temperature of a battery. The following equation represents the energy balance equation that characterizes the thermal distribution within the battery. During the process of battery discharge, the computational domain is analyzed by solving three-dimensional governing equations that account for mass, momentum, and energy conservation. The governing equation for the scenario involving a solid domain, where heat conduction is the only heat transfer mechanism within the cell volume and there is no heat generation, can be expressed as Eq. (7) [9, 15].

$$\rho_b C_{p,b} \left[ \frac{\partial T}{\partial r} \right] = k_s \left[ \frac{\partial^2 T}{\partial x^2} + \frac{\partial^2 T}{\partial y^2} + \frac{\partial^2 T}{\partial z^2} \right] + q_{gen} \qquad (7)$$

The equation Eq. 7 represents the cellular heat production (qgen). The parameters representing the density, specific heat, and thermal conductivity of battery material are conventionally designated as b, $C_{p,b}$, and kf, respectively. The simulation of conjugate heat transfer involves the coupling of the fluid domain, which represents the airflow, with the solid

domain, which accounts for heat conduction and internal volumetric heat generation. A convective boundary condition is frequently employed to simulate the heat exchanger within the BTMS while modeling the system. The velocity intake is assigned to the left side of the battery domain, while the exit is treated as a pressure outlet. In order to regulate temperature, we utilize ambient air at a temperature of 22 °C. In the computational fluid dynamics (CFD) model of the battery pack, the air was represented as a fluid zone, while the battery was represented as a solid zone. The term "coupled wall condition" pertains to the battery surfaces that separate the air zone. The slip boundary requirement does not apply to the limits of the battery. The experimental and commercial software results were validated by employing a sensitivity analysis of the mesh using the numerical free open-source OpenFOAM CFD model.

## 3 Results and discussion

The present study employs OpenFOAM computational fluid dynamics (CFD) software to conduct numerical simulations aimed at investigating the battery drain scenario under the rated current. The establishment of the flow field within the battery module is predicated upon the heat output generated
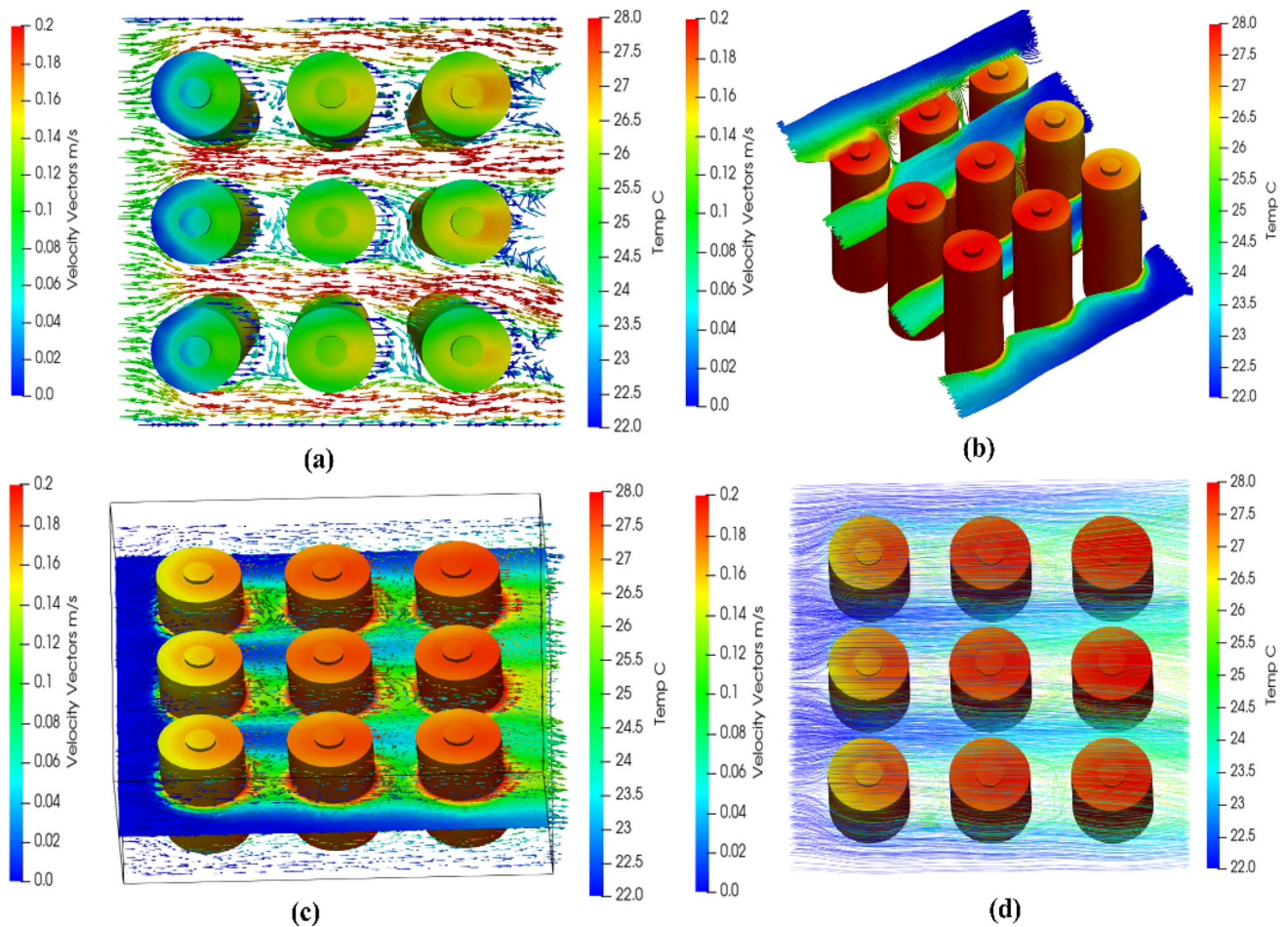
**Fig. 7** Distribution of air and battery cell temperatures at T = 22 °C to 28 °C

by each cell among all the nine cells. The module for transient thermal response provides computational findings that comprise the internal flow field and temperature distribution of the battery module. The generation of heat energy by battery cells can be measured using Eq. (1). During the preliminary phase of the method, the battery cells are kept at a temperature of roughly 22 °C, which nearly aligns with the ambient atmospheric temperature. Figure 6a–d depicts the simulated airflow temperature variation shown in vector representation and surface temperature of the battery, as well as the surrounding air temperatures. Based on the observation depicted in Fig. 6a, it is evident that the temperature and air content of the battery pack exhibit a low value in the initial row at t = 100 S. With sliced views, Fig. 6b depicts the temperature variation of battery cells and air temperature at time t = 50. Figure 6c displays the temperature of both the air and battery cells at t = 500 s, specifically at the midpoint of the battery pack. Figure 6d illustrates a small decrease in the temperature of cells and air temperature at the uppermost region of the battery.

Figure 7a–d displays the temperature profiles of the air employed in the cooling process of the cylindrical battery module at a specific time of t = 500 s. The air velocity is set at 0.1 m/s, and the initial temperature of the air, denoted as Tcell, is 22 °C. Figure 7a illustrates the top view of the battery pack, with the air temperature variations depicted. The battery cell temperature is not presented to provide a clearer representation of the air temperature variations. Figure 7b displays the vertical perspective of air temperature variations in the battery pack. Figure 7c–d presents the vector view and pipeline view of air temperature variation, providing a more comprehensive analysis of the changes in air temperature for enhanced observation. The battery module additionally utilizes ambient air at equivalent temperatures to facilitate efficient operation. The thermal output generated by the module can impact the operational efficiency of the battery.

Figure 8a–f displays the release of heat by cells, where the temperature rises from T = 22 °C to 28 °C at t = 50 s to 500 s. By utilizing the three-dimensional temperature contours depicted in Figs. 7a–f, one can observe the comprehensive temperature ranges and flow patterns within the
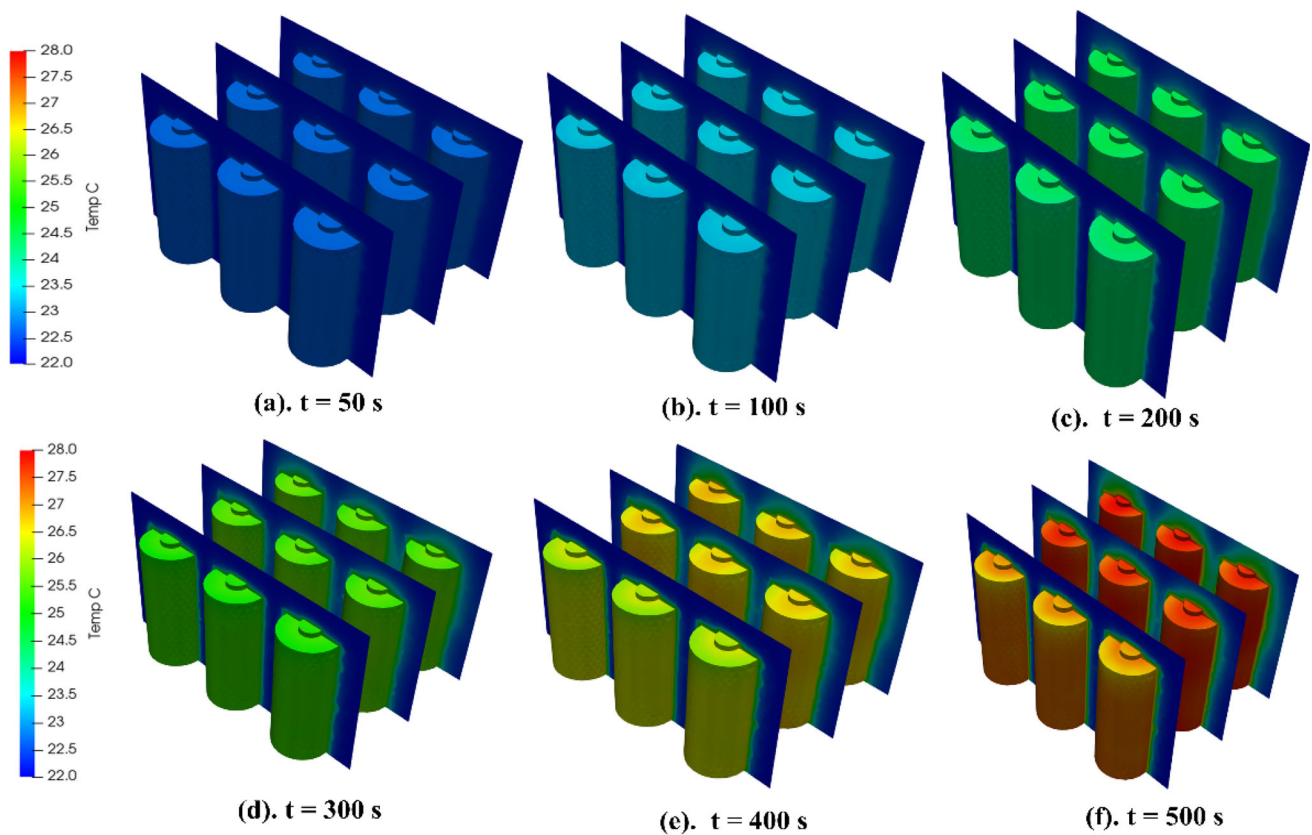
**Fig. 8** Cylindrical cell battery module's transient thermal response at t = 50 s to 500 s and $T_{cell}$ = 22 °C to 28 °C

module at a specific time point of t = 50 s. The cell's output of heat is relatively low during this time. Subsequently, at t = 100 to 300 s, the heat generation gradually increases. The range of cell colors and the elevated temperatures around the cells show that the heat generation finally reaches a high level at t = 400 to 500 s. The temperature distribution in the cells of the first row is marginally lower compared to the cells in the subsequent two rows due to their direct exposure to the input of cool air. The removal of waste heat from the battery module is facilitated by the circulation of cooling air at a reduced supply temperature. The thermal behavior of the battery is primarily influenced by the configuration of the battery cells, the spacing between neighboring cells, and the presence and temperature of cooling fluids.

Figure 9 illustrates the utilization of three-dimensional temperature contours to visually represent the whole range of temperature regimes and flow fields within the module.

The module exhibits evident hotspots and temperature fluctuations. The presence of isolated hotspots undermines the dependability of the battery. In Fig. 9a–d four planes were selected at different heights (h = 25 mm, 5 mm, 75 mm, and 90 mm) in order to investigate localized heat spots. The evaluation was conducted at a discharge time of 500 s with supply air conditions of 22 °C and a velocity of 0.1 m/s. The absence

of any discernible change in air temperature is evident until it reaches the initial row of battery cells. Moreover, it has been shown that the areas adjacent to the module's two lateral walls remain unaffected by the dissipation of heat generated by the cells.

The phrase "local heat spots" is employed to characterize regions when the ambient air temperature is anomalously elevated. Figure 9 displays the temperature contours of the cooling media (air) within the cylindrical battery module. Within the module, there exist localized hotspots situated behind the cells. The acquisition of such data can be facilitated through the implementation of a quantitative evaluation of ambient air temperature within the battery module. Significant temperature variations exist between the regions located behind the cells in the second and first rows. The temperature gradient exhibits variation in relation to the depth of the module, with the most pronounced inclination observed towards the base surface of the module. The detection of modulator air temperature variations allows for the identification of the specific locations where heat is being transferred, specifically from the surface of the battery to the cooling media. The investigation also encompassed the examination of temperature regimes formed across the breadth of the module in the transverse direction. The architecture of the BTMS
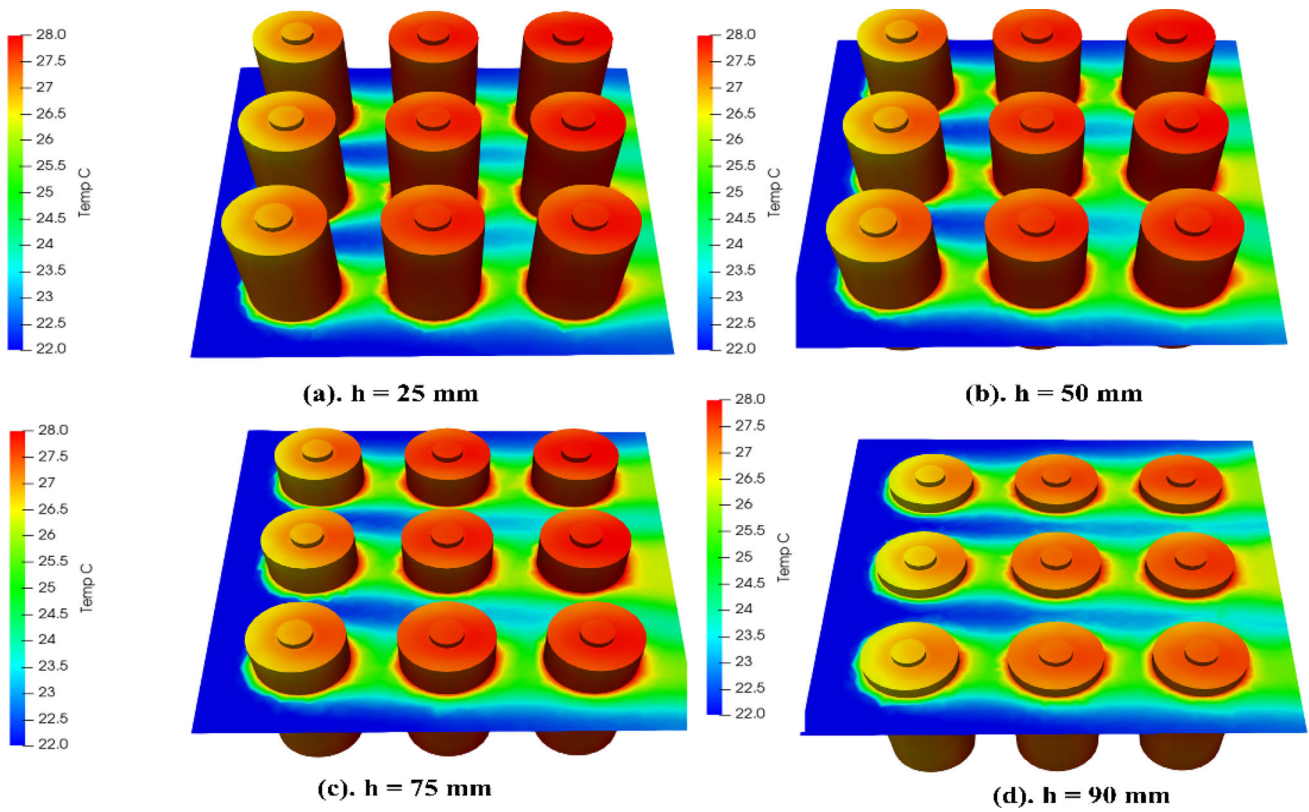
**Fig. 9** The temperature contours of the cooling media inside the battery module at h = 25 mm to 90 mm, t = 500 s Air velocity = 0.1 m/s to 0.5 m/s, $T_{cell}$ = 22 C)
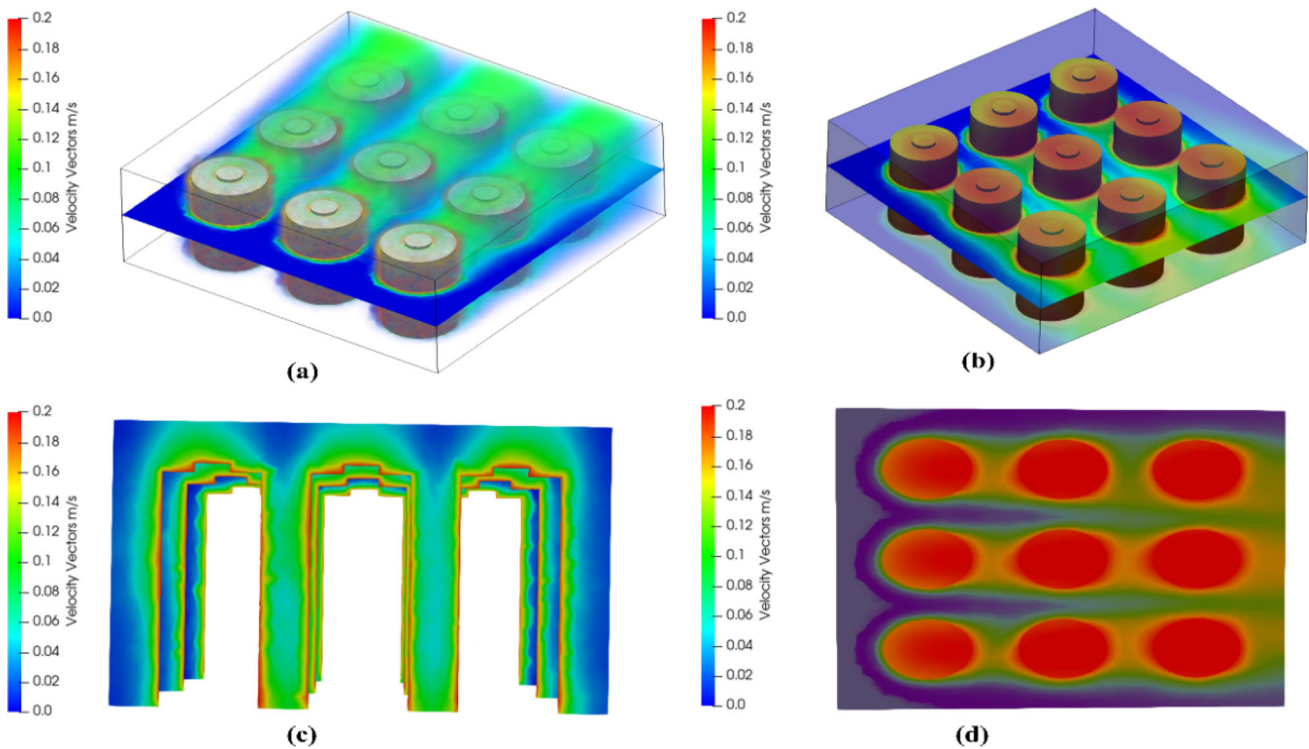


**Fig. 10** Flow field in 3-dimensional, cross-sectional, and top surface views

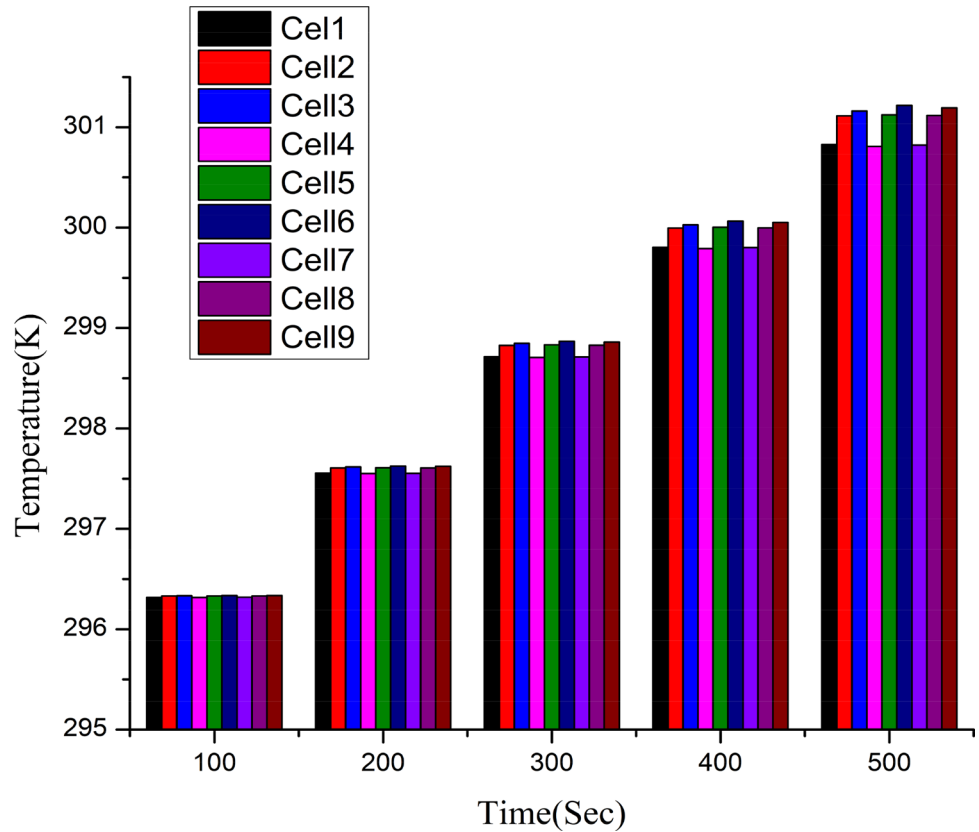**Fig. 11** Temperature distribution of each cell of the battery module (at t = 100 to 500 s)
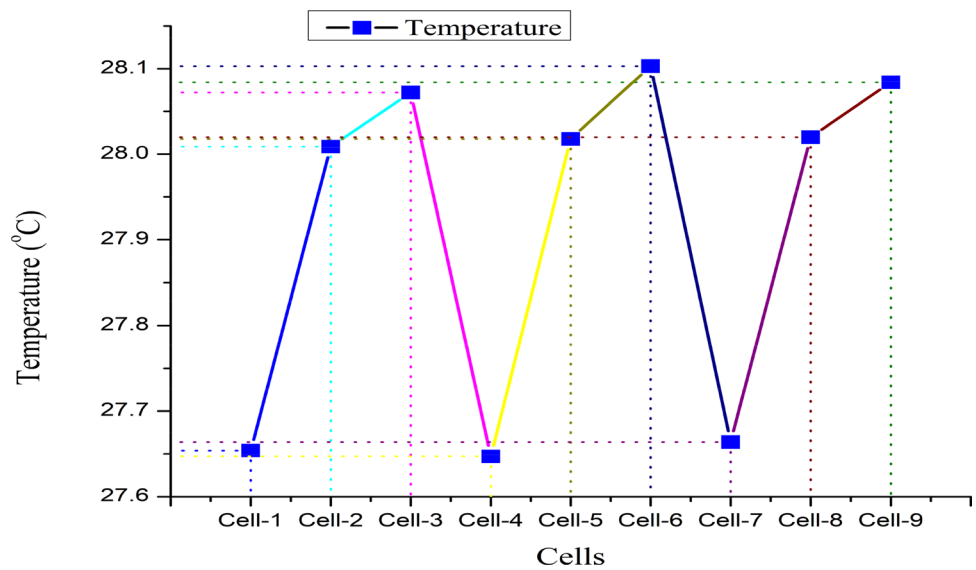


**Fig. 12** Battery pack cell temperature variation (Maximum Temperature at 6th cell)



is significantly dependent on the external flow that traverses the battery cell. Through the process of convection, cells can dissipate surplus heat into their immediate environment.

Figure 10a–b depicts a three-dimensional representation of the cylindrical battery module's air and temperature. Figure 10c presents the cross-sectional depiction of the battery pack, wherein the lack of a battery is observed and the temperature of the surrounding air is measured. The temperature of the air's surface is observed to be increasing at a greater rate than that of the pack's surface.

Figure 10d illustrates the flow field, wherein the air temperature reaches its maximum value between the rows and in proximity to the curvature of the cells. The no-slip boundary condition postulates that the velocity of the air at the surface of the battery is zero. The airflow surrounding the battery

cell undergoes a division at the moment of separation. The resultant boundary layer fully encompasses the cell. When the velocity of air decreases to zero at the stagnation point, there is an associated increase in pressure in that region. An increase in air velocity leads to a reduction in pressure in the direction of airflow. The air velocities exhibit their maximum magnitudes precisely at the locations of cellular gaps. A separation zone is created in the wake of the battery cell when air passes over it and becomes detached from the surface. This detachment occurs in the boundary layer that envelops the cell. The investigation revealed that the occurrence of air recirculation and backflows within the isolation zones exhibited variations corresponding to the depth of the module. The analysis focuses on the examination of airflow patterns within a battery module under specific conditions, namely at a temperature of 22 °C and a supply air velocity of 0.1 m/s. The duration of the discharge is 500 s. The cells located closer to the exit exhibit a somewhat higher temperature compared to their respective preceding cells.

Figure 11 shows the graphical representation of each cell temperature with different periods. At t = 500 s the more variation among all the cells. In all the cells, the cells in row 1, namely those indexed 1, 4, and 7, exhibit a high degree of efficiency in dissipating heat into the surrounding colder air.

Cells located in row 2, specifically those with indices 2, 5, and 8, can collect heat in the direction of their flow and subsequently release it to the surrounding warmer air. Cells located in row 3, specifically those with indices 3, 6, and 9, exhibit the highest air temperature and serve as the primary hot spot among all the cells. Cell 6 exhibits the highest level of thermal energy. By employing the volume-weighted average temperature, it is possible to visually represent the temporal dynamics of the thermal response of the cell. The battery module as a whole is evaluated under ambient conditions, characterized by a moderate flow rate (v = 0.1 m/s) and a temperature of 22 °C. Figure 12 illustrates the individual response of each cell within the battery module, including the transfer of heat between cells. Among all the cells, it is observed that cell 6 experiences a higher level of heat dissipation.

## 4 Conclusions

The increasing demand for electric and hybrid electric vehicles necessitates the development of more efficient battery heat management systems to meet the expectations of EV and HEV consumers. This study employs the OpenFOAM CFD program, which is freely available and open-source, to construct a three-dimensional representation of a cylindrical cell battery pack. Through simulation, we investigate the battery pack's thermal runaway characteristics and examine its flow patterns and heat distributions. The thermal model

incorporating a user-defined function (UDF) is employed to compute the thermal energy generated by the battery. The present study aims to validate the results obtained from Open-FOAM simulations by comparing them with experimental data and results obtained from Ansys simulations as reported in the existing literature. The literature demonstrates that the temperature profile of cell 5 is higher. Research findings have demonstrated that the air temperature profiles within cell 6 exhibit the highest recorded values. The characteristics of cylindrical battery packs differ based on the flow direction as well as the position inside the pack's breadth and depth. As the temperature decreases, the proximity of a module to a cooling air source increases. The cells in the third row of the module exhibit higher temperatures compared to the remaining cells. The air temperature exhibits variations along the direction of flow as well as across the breadth and depth of the module. Observations of transverse temperature gradients in the atmosphere have been made. The presence of localized areas of increased heat is verified when the temperature exceeds the prescribed cooling threshold (22 °C) and reaches a local peak temperature (28.1 °C) at time t = 500 s. The highest local temperatures are primarily located at the geometric center of the last row of the module. The battery module exhibits typical flow characteristics. The battery is composed of multiple layers that exhibit variable levels of flow separation. The temperatures of battery cells undergo variations when they transition from one position to another within the battery module.

## References

1. Haghani, M., Sprei, F., Kazemzadeh, K., Shahhoseini, Z., Aghaei, J.: Trends in electric vehicles research. Transportation Res. Part D: Transp. Environ. **123**, 103881 (2023). https://doi.org/10.1016/j.trd.2023.103881,. (**ISSN 1361-9209**)

2. Timilsina, L., Badr, P.R., Hoang, P.H., Ozkan, G., Papari, B., Edrington, C.S.: Battery degradation in electric and hybrid electric vehicles: a survey study. IEEE Access **11**, 42431–42462 (2023). https://doi.org/10.1109/ACCESS.2023.3271287

3. Aghabali, I., et al.: 800-V electric vehicle powertrains: review and analysis of benefits, challenges, and future trends. IEEE Trans. Transportation Electrif. **7**(3), 927–948 (2021). https://doi.org/10.1109/TTE.2020.3044938

4. Kumar, R.R., Bharatiraja, C., Udhayakumar, K., Devakirubakaran, S., Sekar, K.S., Mihet-Popa, L.: Advances in batteries, battery modeling, battery management system, battery thermal management, SOC, SOH, and charge/discharge characteristics in EV applications. IEEE Access **11**, 105761–105809 (2023). https://doi.org/10.1109/ACCESS.2023.3318121

5. Bukya, M., Kumar, R., Mathur, A.: Analytical computation of thermal and electrical issues in E-mobility cabling network. J. Adv. Res. Fluid Mech. Therm. Sci. **104**(1), 84–92 (2023). https://doi.org/10.37934/arfmts.104.1.8492

6. Jung, C.: Power Up with 800-V systems: the benefits of upgrading voltage power for battery-electric passenger vehicles. IEEE Electrif. Mag. **5**(1), 53–58 (2017). https://doi.org/10.1109/MELE.2016.2644560

7. Hong, J., et al.: Fault prognosis and isolation of lithium-ion batteries in electric vehicles considering real-scenario thermal runaway risks. IEEE J. Emerg. Sel. Top. Power Electron. **11**(1), 88–99 (2023). https://doi.org/10.1109/JESTPE.2021.3097827

8. Bukya, M., et al.: Numerical investigation on thermal and electrical stress in electric vehicle cabling network. J. Adv. Res. Fluid Mech. Therm. Sc. **102**(1), 25–36 (2023)

9. Rao, Z., Wang, S.: A review of power battery thermal energy management. Renew. Sustain. Energy Rev. **15**(9), 4554–4571 (2011)

10. Huaqiang, L., et al.: Thermal issues about Li-ion batteries and recent progress in battery thermal management systems: a review. Energy Convers. Manage. **150**(10), 304–330 (2017)

11. Bukya, M., Kumar, R.: Safety consideration and design of high voltage cable for electric vehicle. In: 2020 International Conference on Power Electronics & IoT Applications in Renewable Energy and its Control (PARC), pp. 485–490. Mathura (2020)

12. Fayaz, H., et al.: Optimization of thermal and structural design in lithium-ion batteries to obtain energy efficient battery thermal management system (BTMS): a critical review. Arch Computat. Methods Eng **29**(4), 1–66 (2021)

13. Jilte, R.D., Kumar, R.: Numerical investigation on cooling performance of Li-ion battery thermal management system at high galvanostatic discharge. Eng. Sci. Tech. Int. J. **21**(5), 957–969 (2018)

14. Voigt, S., Sträubig, F., Palis, S., Kwade, A., Knaust, C.: CFD-analysis of the sensible enthalpy rise approach to determine the heat release rate of electric-vehicle-scale lithium-ion battery fires. Fire Safety J. **114**, 102989 (2020). https://doi.org/10.1016/j.firesaf.2020.102989. (**ISSN 0379-7112**)

15. Abdul, Q., et al.: Heat generation in high power prismatic Li-ion battery cell with $LiMnNiCoO_2$ cathode material. Int. J. Energy Res. **38**(9), 1424–1437 (2014)

16. Muddasar, M.: Optimization, Modelling and Analysis of Air-Cooled Battery Thermal Management System for Electric Vehicles. *Preprints* 2022010051 (2022)

17. Zhang, L., et al.: Cell-to-cell variability in Li-ion battery thermal runaway: experimental testing, statistical analysis, and kinetic modeling. J Energy Storage **56**(Part B), 106024 (2022)

18. Gungor, S., Gocmen, S., Cetkın, E.: A review on battery thermal management strategies in lithium-ion and post-lithium batteries for electric vehicles. J. of Thermal Eng. **9**, 1078–1099 (2023)

19. He, F., et al.: Combined experimental and numerical study of thermal management of battery module consisting of multiple Li-ion cells. Int. J. Heat Mass Transf. **72**(5), 622–629 (2014)

20. Zhao, X.: Thermal performance analysis and optimal control of power lithium cell thermal management system for new energy vehicles. Therm. Sci. **24**(1), 129–129 (2020)

21. Mills, A., Al-Hallaj, S.: Simulation of passive thermal management system for lithium-ion battery packs. J. Power Sour. **141**(2), 307–315 (2005)

22. Wang, S., et al.: Experimental exploration of finned cooling structure for the thermal management of lithium batteries with different discharge rate and materials. Therm. Sci. **24**(1), 69–69 (2019)

23. Li, X., et al.: Thermal management of cylindrical batteries investigated using wind tunnel testing and computational fluid dynamics simulation. J. Power Sour. **238**(9), 395–402 (2013)

24. Tuğan, V., Yardımcı, U.: Numerical study for battery thermal management system improvement with air channel in electric vehicles. J. Energy Storage **72**(Part C), 108515 (2023). https://doi.org/10.1016/j.est.2023.108515. (**ISSN 2352-152X**)

25. Ruijia, F.: Numerical study on the effects of battery heating in cold climate. J. Energy Storage **26**(12), 100969 (2019)

26. Zheng, D., et al.: Heat transfer performance and friction factor of various nanofluids in a double-tube counter flow heat exchanger. Thermal Sci. **24**(1), 280–280 (2020)

27. Sundin, D.W., Sponholtz, S.: Thermal management of Li-Ion batteries with single-phase liquid immersion cooling. IEEE Open J. Veh. Technol. **1**, 82–92 (2020). https://doi.org/10.1109/OJVT.2020.2972541

28. Singh, L.K., Bhadauria, A., Srinivasan, A., Pillai, U.T.S., Pai, B.C.: Effects of gadolinium addition on the microstructure and mechanical properties of Mg–9Al alloy. Int. J. Miner. Metall. Mater. **24**, 901–908 (2017)

29. Sun, Z., Guo, Y., Zhang, C., Xu, H., Zhou, Q., Wang, C.: A novel hybrid battery thermal management system for prevention of thermal runaway propagation. IEEE Trans. Transportation Electrif. (2023). https://doi.org/10.1109/TTE.2022.3215691

30. Dinbandhu, Prajapati, V., Vora, J.J. et al.: Experimental studies of regulated metal deposition (RMD (TM)) on ASTM A387 (11) steel: study of parametric influence and welding performance optimization. J. Braz. Soc. Mech. Sci. Eng. **42**, 78 (2020). https://doi.org/10.1007/s40430-019-2155-3

31. Wang, R., Liang, Z., Souri, M., Esfahani, M.N., Jabbari, M.: Numerical analysis of lithium-ion battery thermal management system using phase change material assisted by liquid cooling method. Int. J. Heat Mass Transfer **183**(Part B), 122095 (2022). https://doi.org/10.1016/j.ijheatmasstransfer.2021.122095. (**ISSN 0017-9310**)

32. Shelly, T.J., Weibel, J.A., Ziviani, D., Groll, E.A.: Comparative analysis of battery electric vehicle thermal management systems under long-range drive cycles. Appl. Thermal Eng. **198**, 117506 (2021). https://doi.org/10.1016/j.applthermaleng.2021.117506. (**ISSN 1359-4311**)

33. Parsons, K.K., Mackin, T.J.: Design and simulation of passive thermal management system for lithium-ion battery packs on an unmanned ground vehicle. ASME. J. Thermal Sci. Eng. Appl. **9**(1), 011012 (2016). https://doi.org/10.1115/1.4034904

34. Bhadauria, A., Bajpai, S., Tiwari, A., Mishra, S.K., Nisar, A., Dubey, S., et al.: Bimodal microstructure toughens plasma sprayed Al2O3-8YSZ-CNT coatings. Ceram. Int. **49**(8), 12348–12359 (2023)

35. Murali Mohan, M., Venugopal Goud, E., Deva Kumar, M. L. S., Kumar, V., Kumar, M., Dinbandhu.: Parametric optimization and evaluation of machining performance for aluminium-based hybrid composite using utility-Taguchi approach. In: Recent Advances in Smart Manufacturing and Materials: Select Proceedings of ICEM 2020, pp. 289–300. Springer, Singapore (2021)

36. Afzal, A., Kaladgi, A.R., Jilte, R.D., Ibrahim, M., Kumar, R., Mujtaba, M.A., Alshahrani, S., Saleel, C.A.: Thermal modelling and characteristic evaluation of electric vehicle battery system.

Case Studies in Thermal Engineering **26**, 101058 (2021). https://doi.org/10.1016/j.csite.2021.101058. (**ISSN 2214-157X**)

37. Mi, C., Li, B., Buck, D., Ota, N.: Advanced electro-thermal modeling of lithium-ion battery system for hybrid electric vehicle applications. In: 2007 IEEE Vehicle Power and Propulsion Conference, Arlington, TX, USA, pp. 107–111. https://doi.org/10.1109/VPPC.2007.4544108 (2007)

38. Al Qubeissi, M., Mahmoud, A., Al-Damook, M., Almshahy, A., Khatir, Z., Soyhan, H.S., Raja Ahsan Shah, R.M.: Comparative analysis of battery thermal management system using biodiesel fuels. Energies **16**, 565 (2023)

39. Yang, Z., Patil, D., Fahimi, B.: Electrothermal modeling of lithium-ion batteries for electric vehicles. IEEE Trans. Veh. Technol. **68**(1), 170–179 (2019). https://doi.org/10.1109/TVT.2018.2880138

40. Bukya, M., Meenakshi Reddy, R., Atchuta Ramacharyulu, D., Kumar, R., Mathur, A., Gupta, M., Garimella, A.: Electro-thermal performance evaluation of a prismatic battery pack for an electric vehicle. High Temp. Mater. Proc. **43**, 20220311 (2024)

41. Bukya, M., Malthesh, S., Kumar, R., Mathur, A.: Insulation detection of electric vehicles by using FPGA-based recursive-least-squares algorithm. World Electr. Veh. J. **15**(1), 25 (2024). https://doi.org/10.3390/wevj15010025

42. Bukya, M., Sharma, S., Kumar, R., Mathur, A., Gowtham, N., Kumar, P.: Electric vehicle grid demand potential analysis model and regional architectural planning approach for charging using PVsyst tool. Visions Sustain. **21**(8869), 1–24 (2024)

43. Bukya, M., Kumar, R., Mathur, A.: Electrical vehicles insulation detection using Virtex 7 FPGA. In: Innovations in Computational Intelligence and Computer Vision. ICICV 2022. Lecture Notes in Networks and Systems, vol 680. Springer, Singapore. https://doi.org/10.1007/978-981-99-2602-2_57

44. Bukya, M., Kumar, R., Gupta, R.K.: A study on safety issues and analytical evaluation of stresses for HVDC cable in electrical vehicle. In: AIP Conf. Proc. 22 Dec 2020, vol. 2294, No. 1, p 040001. https://doi.org/10.1063/5.0031351 (2020)